Raman scattering and optical-absorption studies of the metastable alloy system $GaAs_xSb_{1-x}$

T. C. McGlinn, T. N. Krabach, and M. V. Klein
Physics Department and Materials Research Laboratory, University of Illinois at Urbana-Champaign, 104 South Goodwin Avenue, Urbana, Illinois 61801

G. Bajor,* J. E. Greene, B. Kramer, S. A. Barnett,† A. Lastras,‡ and S. Gorbatkin
Department of Metallurgy, Coordinated Science Laboratory, and Materials Research Laboratory, University of Illinois at Urbana-Champaign, 1101 West Springfield Avenue, Urbana, Illinois 61801
(Received 2 December 1985)

The optical properties of $GaAs_xSb_{1-x}$ alloys grown across the entire concentration range by multitarget sputter deposition are reported. X-ray diffraction, optical absorption, and Raman spectra show the samples to be single-crystal, single-phase alloys for all x, including those in the miscibility gap. Alloy lattice constants are found to vary linearly with concentration. The direct Γ-point energy gaps, determined from optical-absorption measurements, show significant negative bowing. Contrary to previous reports, the Raman spectra exhibit two-mode behavior throughout, including a local mode of As in GaSb and a resonant mode of Sb in GaAs. An analysis of peak frequencies and line shapes versus concentration is given in the context of disorder effects. We observe broadenings much less severe and asymmetric than those seen in similar systems and usually interpreted in terms of $\mathbf{k}\neq\mathbf{0}$ density-of-states activation. The observed adherence to *zone-center* selection rules for all x, suggests a more accurate interpretation to be one involving the $\mathbf{k}\approx\mathbf{0}$ spectral projection of the density of states.

I. INTRODUCTION

Optoelectronics applications have generated widespread interest in pseudobinary III-V alloys. In particular, the GaAs-GaSb system is of interest for the fabrication of sources and detectors in the ≥ 1-μm wavelength range for fiber-optics communications. Photodiodes,[1] photocathodes,[2] light-emitting diodes,[3] and double-heterostructure lasers[4] with $GaAs_xSb_{1-x}$ active layers have been reported. Most of these devices utilize layers with low GaSb mole fraction. Gratton *et al.*[5] have reported a miscibility gap extending from $x=0.30$ to 0.62 at the peritectic temperature 746 °C. The miscibility gap was found to increase with decreasing temperature and ranged from ~ 0.2 to 0.9 at 600 °C. Thus $GaAs_xSb_{1-x}$, in addition to practical applications, is of fundamental interest in the study of nonequilibrium crystal growth.[6,7]

Most optical measurements[8–11] have thus far been restricted to the end-point concentration regions. Included among these are phonon studies[12] reporting a "one-two" type of mode behavior; specifically, the existence of two optic-phonon modes at the GaSb-rich end and only one mode at the GaAs-rich region (i.e., no local mode of Sb in GaAs). This observation was attributed to the lack of a gap in the GaAs one-phonon density of states, the Sb local mode thus being damped out. The observation of two modes in the GaSb-rich alloys included a GaAs local mode at about 240 cm^{-1}.

Nonequilibrium vapor-phase–growth techniques including molecular-beam epitaxy[13] (MBE) and organometallic chemical-vapor deposition[14] (OMCVD) have been used to grow $GaAs_xSb_{1-x}$ at compositions and temperatures within the miscibility gap. No optical characterization has been reported for the MBE films, although Cherng *et al.*[15] used optical absorption in measuring the room-temperature band gap E_0 for OMCVD $GaAs_{0.5}Sb_{0.5}$ to be 0.77 eV. Recently, Cohen *et al.*[16] reported Raman and photoluminescence results for OMCVD $GaAs_xSb_{1-x}$ alloys with $0<x<0.6$. Phonon line shapes from alloys near the center of the miscibility gap showed severe asymmetric broadenings which were attributed to compositional fluctuations.

Greene and co-workers[6,7] have developed vapor-phase–growth techniques which operate under conditions even further removed from thermal equilibrium than MBE and OMCVD. The key feature in this work is the use of low-energy-ion bombardment of the film surface during deposition. "Low energy" in this context refers to energies with a corresponding ion range of the order of 1–2 monolayers. As discussed in recent review articles,[17,18] low-energy-ion bombardment results in large changes in film nucleation and growth kinetics, near-surface diffusivities, and elemental incorporation probabilities. This has allowed, for example, the growth of single crystal $(A^{III}B^{V})_{1-x}(C_2^{IV})_x$ alloys, which exhibit essentially no solid solubility, at x values ranging from 0 to 1. In the present experiments, the primary role of the low-energy-ion irradiation is to provide dynamical collisional mixing of the upper one or two layers during film growth.

In this paper, we present Raman scattering and optical-absorption results from $GaAs_xSb_{1-x}$ films grown on GaAs(100) substrates by multitarget rf sputtering[19] with an induced negative bias on the growing film to facilitate ion bombardment. Alloys were grown at compositions spanning the entire pseudobinary phase diagram.

The lattice constants are shown to obey Vegard's law while the room-temperature optical band gap $E_0(x)$ exhibits negative parabolic bowing in agreement with previous results. On the other hand, the present Raman results show two-mode behavior, in contrast to the "one-two" type of mode behavior previously reported for this system. In addition, the measured Raman peak broadening and asymmetry is much less than that observed in recent studies of microcrystalline Si,[20] $Al_xGa_{1-x}As$,[21,22] $(GaSb)_{1-x}(Ge_2)_x$,[23] and ion-implanted GaAs.[24] The usual view is that alloy or structural disorder relaxes the $k \approx 0$ (momentum) conservation rule, allowing modes away from the Brillouin-zone center to contribute to light scattering. Our results suggest a refinement to this interpretation.

II. EXPERIMENTAL PROCEDURE

The $GaAs_xSb_{1-x}$ films were grown in a multitarget rf sputtering system with a differentially pumped sample load lock. The system has been described in detail previously[25] and only the essential features will be noted here. The base pressure during these experiments was better than 10^{-7} Torr while the Ar pressure during deposition was 15 mTorr. The Ar sputtering gas had an initial purity of 99.9999% and was further purified by passing it through a Ti-sponge getter at 900 °C prior to introducing it into the sputtering chamber. The induced negative potential on the substrate with respect to the positive space-charge potential in the plasma was 75 V.

The source material for film growth was supplied by two 10-cm-diam targets, GaAs and either GaSb or $GaAs_{0.3}Sb_{0.7}$, each with a purity of better than 99.999%. Separate continuous discharges were established under each target while the substrate platter was rotated through the discharges at programmed rates. The target voltages ranged from 350 to 1200 V to provide deposition rates between 0.1 and 0.9 monolayers per target pass. The total film thicknesses were 1–2.5 μm. An excess group-V vapor pressure during deposition was provided by evaporating 99.9999%-pure As from an effusion cell aimed at the growing film.

Undoped semi-insulating GaAs(100) wafers were used as substrates. The cleaning and substrate preparation has been described previously.[25] The final step consisted of sputter-etching the wafers at 570 °C in a 250-V, 5-mTorr Ar discharge. The films were grown at temperatures ranging from 450 to 600 °C. Film composition was determined by wavelength-dispersive x-ray-energy analysis (EDX) using elemental reference standards and the Magic V computer program to carry out matrix corrections. X-ray diffraction and electron microscopy were used to investigate the crystalline perfection of the as-deposited films and optical absorption was measured in order to determine the room-temperature band gap as a function of composition.

Raman spectra were obtained using the 5145-Å line from an Ar-ion laser at Brewster-angle incidence. The backscattered light was analyzed using a rotating polaroid filter and a double monochromator with 2-cm^{-1} resolution before being detected by conventional photon-counting electronics. Spectra were taken with [100] and [110] incident polarizations. Parallel and perpendicular polarizations were analyzed separately.

III. EXPERIMENTAL RESULTS AND DISCUSSION

A. Film composition

The alloy composition was controlled by adjusting the target sputtering rate S, the As effusion-cell temperature T_e, and the film-growth temperature T_s based upon established calibration curves. The Sb concentration increased with increases in S and T_s and decreases in T_e. The Sb desorption rate coefficient, and hence the Sb surface binding energy, was found to be strongly dependent on the As surface coverage.

All films were (100)-oriented single crystals as deduced by electron microscopy and x-ray diffraction (XRD) studies. Electron-channeling patterns exhibited sharp high-order reflections with no indication of either high- or low-angle grain boundaries as the electron beam was scanned over the entire surface of the samples. The lattice constant of $GaAs_xSb_{1-x}$, as determined from fundamental (400) XRD reflections, is shown in Fig. 1 as a function of $1-x$. The results are in good agreement with Vegard's law as well as with previous MBE data.[13]

B. Optical-absorption measurements

The direct Γ-point band gap E_0 was determined as a function of alloy composition from optical-absorption measurements carried out over the wavelength range from 0.9 to 2.5 μm. The data were fitted using the usual "three-layer"[26] model, which requires the thickness t and the refractive index n of the film. t was obtained from the separation of the interference fringes and was in reasonable agreement with calibrated deposition rate

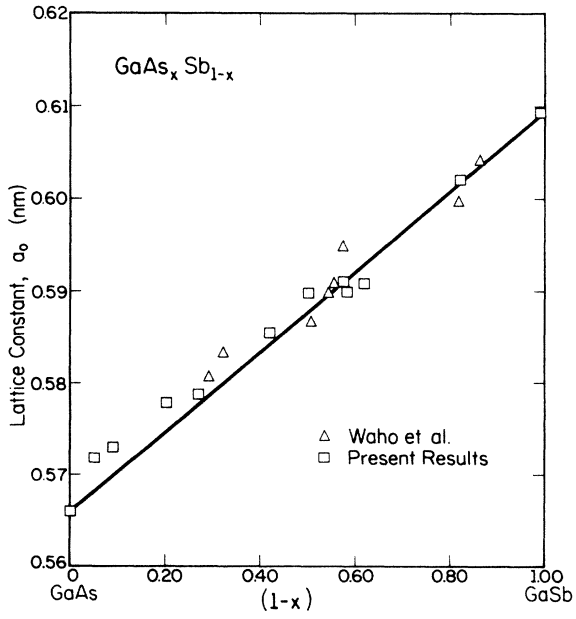

FIG. 1. Lattice constant as a function of Sb concentration for $GaAs_xSb_{1-x}$.

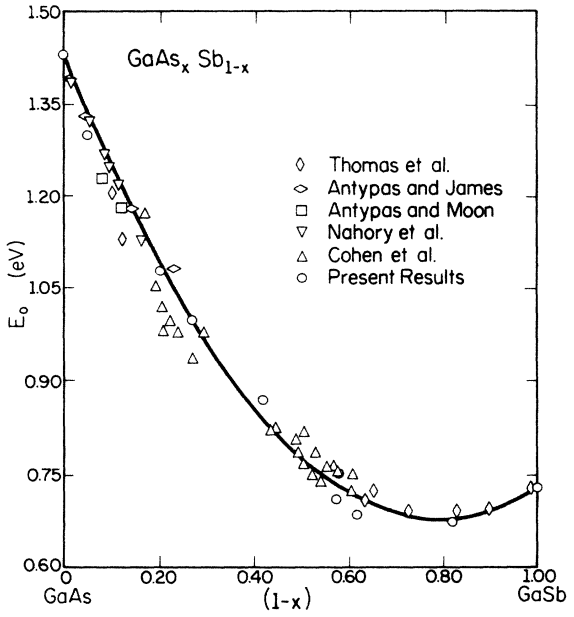

FIG. 2. Room-temperature direct-band-gap energy E_0 as a function of Sb concentration.

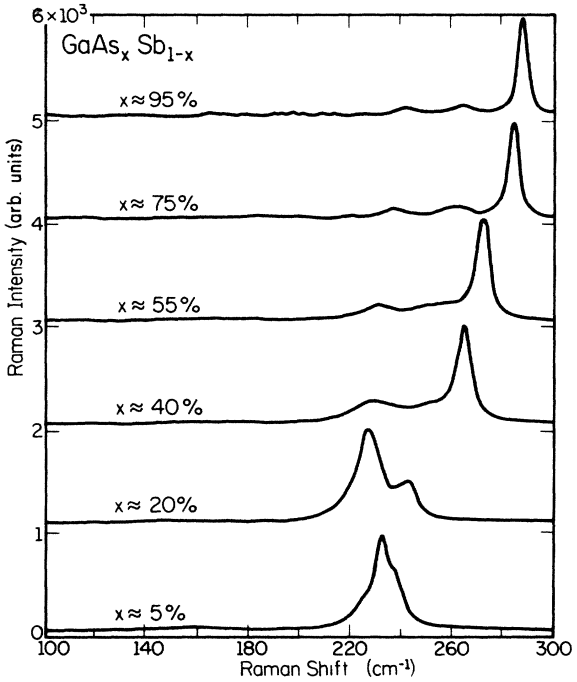

FIG. 3. Representative sampling of room-temperature Raman spectra of $GaAs_xSb_{1-x}$. Scattering geometry: $z(x,y)\bar{z}$ (all normalized to same maximum peak height).

curves. The refractive index of each film was determined in the low-absorption region and then fitted over the entire wavelength range with a quadratic dependence on wavelength. The direct band gap E_0 was obtained by fitting the absorption coefficient α to an expression of the form[27] $\alpha \sim (h\nu - E_0)^{1/2}$. E_0 versus x was found to exhibit a negative bowing as shown in Fig. 2. The present data are in good agreement with previous measurements[16] as well as calculated results[8] based on the dielectric model of Van Vechten and Bergstresser.[28]

C. Raman scattering

Raman scattering is a sensitive local probe. As such, it has developed into a popular and effective tool for characterizing disorder in semiconductors.[29] This usually involves a study of optic-mode frequencies and line shapes. Shown in Fig. 3 is a representative sampling of our Raman spectra, taken in a $z(x,y)\bar{z}$ configuration—backscattering off a [001] face with ϵ_i along [100] and ϵ_s along [010]—an allowed geometry for scattering by zone-center longitudinal-optical (LO) phonons in a zinc-blende lattice. The prominent features in this frequency range are due to first-order scattering from both "GaSb-like" and "GaAs-like" modes. Weak, symmetry-forbidden transverse-optic– (TO-) mode scattering was observed due to our imperfect backscattering geometry. Contrary to previous works,[12] we observe two-mode behavior over the entire concentration range, including local modes of As in GaSb and resonant modes of Sb in GaAs. Starting at the GaAs-rich end, our spectra show nicely the continuous shifting and broadening of the "GaAs-like" mode as it devolves, upon substitution by Sb, into a local mode at about 240 cm^{-1}. Concurrently, we can track the evolution of the "GaSb-like" mode from a mode at 242 cm^{-1}—resonant with the zone-edge LO modes of GaAs. The "GaSb-like" mode exhibited much less scattering strength, which may account for the failure of previous studies to detect the GaSb resonant mode. We see no scattering due to compositional clustering or phase segregation.

In Fig. 4 we give a plot of peak frequencies versus concentration showing classic two-mode behavior for the optic phonons throughout the concentration range. The LO-TO splitting of the "GaSb-like" mode could not be resolved for $x > 0.30$ due to broadening. Also plotted are the center frequencies of weak, broad features observed at lower energies and attributed to disorder-activated scattering by longitudinal-acoustic (DALA) and transverse acoustic (DATA) phonons.[21,30] These too are seen to shift continuously from one endpoint to the other.

Figure 5 illustrates an important point; the adherence of the dominant scattering to *zone-center* selection rules, even in the most disordered case. In this spectrum (incident polarization along [100]), both the allowed [010] and forbidden [100] scattered polarizations are shown. Only weak, diffuse scattering is seen in the forbidden polarization. This was true for all x and both cases of incident polarization ([100] and [010])—exhibiting true zone-center (T_2) symmetry for the dominant scattering.

In this system, the "GaAs-like" LO-mode scattering is stronger and further separated from the TO mode than its "GaSb-like" counterpart—making a line-shape analysis much easier. The width Γ and asymmetry Γ_a/Γ_b (ratio of the two half widths) of this mode, as a function of concentration, is seen in Fig. 6. The asymmetry (maximum $\approx$ 1.3) is consistently and significantly lower than that re-

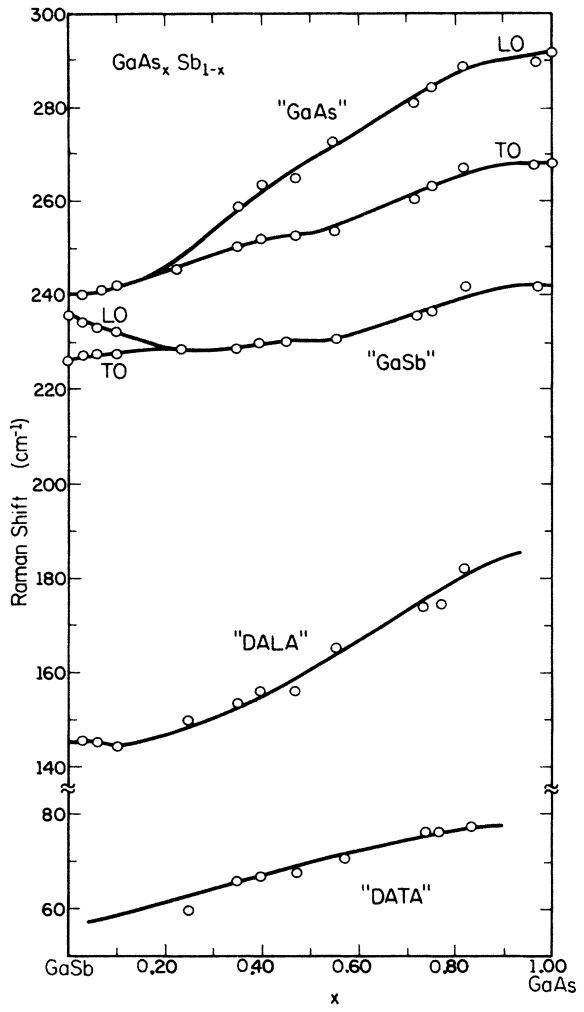

FIG. 4. Frequency dependence of Raman peaks in $GaAs_xSb_{1-x}$ as a function of As concentration. Solid lines are guides to the eye.

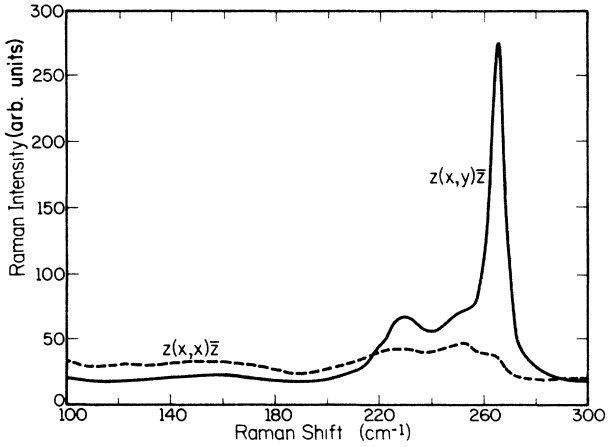

FIG. 5. Typical Raman spectrum for $GaAs_xSb_{1-x}$ showing dependence on polarization of scattered light ($x=0.40$).

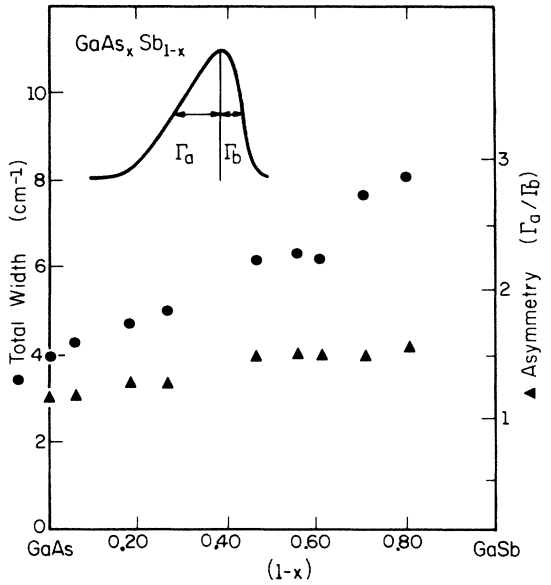

FIG. 6. Asymmetry (Γ_a/Γ_b) and full width at half maximum ($\Gamma=\Gamma_a+\Gamma_b$) of "GaAs-like" longitudinal-optic mode as a function of Sb concentration for $GaAs_xSb_{1-x}$.

ported for the GaAs mode in $Al_xGa_{1-x}As$ (maximum ≈ 2.0)— unexpected by present models. As mentioned, these models account for asymmetric broadening in disordered alloys by allowing the lower-energy modes away from $k\approx 0$ to scatter light. The scattered light from each mode k, is assumed to be Lorentzian with half width $\Gamma(k)$. Assuming a dispersion $\omega(k)$ for the LO mode of the ordered alloy, the Raman intensity is written as a weighted sum of these lines:

$$I(\omega)\alpha \int d\mathbf{k}\, P(k)/\{[\omega-\omega(k)]^2+\Gamma(k)^2\}\ ,$$

where the weighting function $P(k)$ usually involves a phenomenological correlation length. The various models can differ in the choice of weighting functions, dispersion, and half widths. As Jusserand and Sapriel[21] remarked, "this model, while questionable, has the credit of simplicity and can account for the asymmetric broadening of the 'GaAs-like' LO mode in $Al_xGa_{1-x}As$." It cannot, however, simultaneously account for, or predict, the significantly less asymmetry of the same mode in $GaAs_xSb_{1-x}$ nor the sharp changes in the extreme, asymmetric broadenings found in $(GaSb)_{1-x}$ $(Ge_2)_x$.[23] Furthermore, the view of simply activating $k\neq 0$ modes is somewhat misleading, for k is no longer a good quantum number of the disordered alloy. Our observation of *zone-center* selection rules for the dominant scattering, even in the most disordered alloys, implies that a more accurate interpretation of light scattering in mixed crystals involves the $k\approx 0$ projection of the normal modes as discussed below.

IV. THEORY OF RAMAN SCATTERING IN MIXED CRYSTALS

In zinc-blende mixed crystals, one observes coexistence of two types of Raman spectra: (1) relatively narrow peaks at the LO- and TO-phonon frequencies of the

mixed crystal, obeying the usual Raman selection rules, and (2) broad, disorder-activated spectral features often associated with zone-edge phonons. We sketch here a theoretical argument for both types of spectra

In the harmonic approximation, randomness due to atomic disorder affects Raman scattering through randomly varying atomic masses, interatomic force constants, and polarizabilities. These effects were discussed systematically by Lacina and Pershan[31] for the case of $Ca_{1-x}Sr_xF_2$. They gave expressions for the Raman intensity in terms of the polarizability derivatives $\mathbf{p}$ (expressed as a vector with indices that refer to lattice site, atomic position in the unit cell, and Cartesian coordinate) and Green's-function matrix $\mathbf{G}=(\mathbf{M}\omega^2-\mathbf{\Phi})^{-1}$. Here $\mathbf{M}$ is the mass matrix and $\mathbf{\Phi}$ is the force-constant matrix. The intensity is given by

$$\mathrm{Im}(\omega)\sim[1+n(\omega)]\mathrm{Im}\{\langle \mathbf{p}^t\mathbf{G}\mathbf{p}\rangle\}\ , \tag{1}$$

where I means "imaginary part of," and ω is assumed to have a positive infinitesimal imaginary part. $\mathbf{p}^t$ is the transpose of $\mathbf{p}$, $n(\omega)$ is the Bose factor, and the angular brackets denote a configurational average over the disorder.

When the electronic disorder is relatively weak, $\mathbf{p}$ can be approximated by $\mathbf{p}_0\equiv\langle\mathbf{p}\rangle$. The factor in curly brackets in Eq. (1) then becomes

$$\{\cdots\}\approx\mathbf{p}_0^t\mathbf{G}_a\mathbf{p}_0\ , \tag{2}$$

where $\mathbf{G}_a\equiv\langle\mathbf{G}\rangle$. By definition, the quantity $\mathbf{p}_0$ is the polarizability derivative of the virtual crystal. It possesses translational invariance and its use leads to the usual Raman polarization selection rules for a perfect crystal.[32] Equations (1) and (2) give

$$I(\omega)\sim[1+n(\omega)]\mathbf{p}_0^t(\mathrm{Im}\mathbf{G}_a)\mathbf{p}_0\ . \tag{3}$$

The average Green's function $\mathbf{G}_a$ also possesses translational invariance. It is accessible to calculation, for instance, by use of the coherent-potential approximation (CPA).[33,34] For crystal structures that have only one Raman-active mode, such as CaF_2 or zinc-blende, the imaginary part of $\mathbf{G}_a$, when projected onto $\mathbf{p}_0$ as required by Eq. (3), will yield an expression proportional to the spectral density of the Raman-active mode of zero wave vector.[32] That spectrum will have one or two peaks according to whether the mixed crystal in question shows respectively one- or two-mode behavior. It is this leading term in the expansion of Eq. (1) that explains the dominant, relatively narrow LO- and TO-phonon features in mixed crystals.

When electronic disorder cannot be neglected, we must include the effects of a nonzero $\delta\mathbf{p}\equiv\mathbf{p}-\mathbf{p}_0$. It is also convenient to define $\delta\mathbf{G}\equiv\mathbf{G}-\mathbf{G}_a$. The remaining terms in the curly brackets of Eq. (1) then take the form

$$\delta\{\cdots\}=\mathbf{p}_0^t\langle\delta\mathbf{G}\,\delta\mathbf{p}\rangle+\langle\delta\mathbf{p}^t\delta\mathbf{G}\rangle\mathbf{p}_0 +\langle\delta\mathbf{p}^t(\mathbf{G}_a+\delta\mathbf{G})\delta\mathbf{p}\rangle\ . \tag{4}$$

These terms lead to defect-activated Raman scattering from practically all phonon modes. Their contributions to the spectrum will crudely mimic the phonon density of states. The correlations between $\delta\mathbf{G}$ and $\delta\mathbf{p}$ will be localized in space but difficult to model. The $\mathbf{G}_a$ part of the third term in Eq. (4) will be easier to calculate. It involves a correlation between $\delta\mathbf{p}^t$ and $\delta\mathbf{p}$. For a random alloy this correlation will be zero unless the relevant indices for $\delta\mathbf{p}^t$ and $\delta\mathbf{p}$ refer to bonds in the same or adjacent unit cells. The relevant components of $\mathbf{G}_a$ appearing in Eq. (4) will then be diagonal or nearly diagonal on the unit-cell index. Since $\mathbf{G}_a$ is translationally invariant, its eigenstates have well-defined wave vectors. Because of its δ-function-like spatial dependence, the relevant part of $\mathrm{Im}\mathbf{G}_a$ resulting from Eqs. (1) and (4) will bring in the spectral densities of eigenstates belonging to essentially all wave vectors. These are most numerous at the zone edge. This explains the appearance of DALA and DATA spectral features with peaks associated with the zone edge.

V. SUMMARY

We have presented optical-absorption and Raman scattering results for $GaAs_xSb_{1-x}$ alloys grown across the entire concentration range by sputter deposition. Our study shows them to be single crystal, single phase for all x, including those in the miscibility gap. The optical absorption shows the predicted parabolic bowing of E_0 and agrees with available data. The Raman spectra show this alloy to be two-moded throughout—contrary to previous reports of mixed-mode behavior. In addition, the LO-phonon line shapes exhibited less asymmetric broadening than observed in similar systems. Our study of disorder-induced scattering, in terms of phonon line broadening and selection rules, supports the idea of the dominant scattering involving the $k\approx0$ spectral projection of eigenstates of the disordered alloy. Finally, we outlined the Green's-function formalism with which we can explain, qualitatively, the disorder-induced features of our Raman spectra.

ACKNOWLEDGMENTS

This work was supported by the National Science Foundation under Grant No. DMR-83-16981 and the U.S. Joint Services Electronics Program under Contract No. N00014-84-C-0149.

*Present address: Harris Semiconductor, P.O. Box 883, Melbourne, FL 32901.

†Present address: Department of Physics and Measurement Technology, Linköping University, S-581 83 Linköping, Sweden.

‡Present address: Departamento de Física, Unversidad de San Louis Potoci, San Louis Portici, Mexico.

[1]T. P. Pearsal, R. E. Nahory, and M. A. Pollack, Appl. Phys. Lett. **28**, 403 (1976).

[2]G. A. Antypas and L. W. James, J. Appl. Phys. **41**, 2165 (1970); G. A. Antypas, L. W. James, and J. J. Vebbing, *ibid.* **41**, 2888 (1970).

[3]A. Y. Cho, H. C. Casey, Jr., and P. W. Foy, Appl. Phys. Lett. **30**, 397 (1977).

[4]R. E. Nahory and M. A. Pollack, Appl. Phys. Lett. **27**, 562 (1975).

[5]M. F. Gratton, R. C. Goodchild, L. Y. Juravel, and J. C. Woolley, J. Electron. Mater. **8**, 25 (1979).
[6]J. E. Greene, J. Vac. Sci. Technol. **1**, 229 (1983).
[7]S. A. Barnett. B. Kramer, L. T. Ramano, S. I. Shah, M. A. Ray, S. Fang, and J. E. Greene, in *Layered Structures, Epitaxy, and Interfaces,* edited by J. M. Gibson and L. R. Dawson (North-Holland, Amsterdam, 1985), p. 285.
[8]M. B. Thomas, W. M. Coderre, and J. C. Woolley, Phys. Status Solidi A **2**, K141 (1970).
[9]G. A. Antypas and L. W. James, J. Appl. Phys. **41**, 2165 (1970).
[10]R. E. Nahory, M. A. Pollack, J. C. Dewinter, and K. M. Williams, J. Appl. Phys. **48**, 1607 (1977).
[11]G. A. Antypas and P. L. Moon, J. Electrochem. Soc. **121**, 416 (1974).
[12]G. Lucovsky and M. F. Chen, Solid State Commun. **8**, 1397 (1970).
[13]T. Waho, S. Ogawa, and S. Maruyama, Jpn. J. Appl. Phys. **16**, 1875 (1979)
[14]G. B. Stringfellow and J. M. Cherng, J. Cryst. Growth **64**, 413 (1983).
[15]M. J. Cherng, R. M. Cohen, and G. B. Stringfellow, J. Electron. Mater. **13**, 799 (1984).
[16]R. M. Cohen, M. J. Cherng, R. E. Benner, and G. B. Stringfellow, J. Appl. Phys. **57**, 15 (1985).
[17]J. E. Greene and S. A. Barnett, J. Vac. Sci. Technol. **21**, 285 (1982).
[18]J. E. Greene, CRC Crit. Rev. Solid State Mater. Sci. **II**, 47 (1983); **II**, 189 (1984).
[19]C. E. Wickersham and J. E. Greene, J. Appl. Phys. **47**, 4734 (1976).
[20]H. Richter, Z. P. Wang, and L. Ley, Solid State Comm. **39**, 625 (1981).
[21]B. Jusserand and J. Sapriel, Phys. Rev. B **24**, 7194 (1981).
[22]P. Parayanthal and F. H. Pollak, Phys. Rev. Lett. **52**, 1822 (1984).
[23]R. Beserman, J. E. Greene, M. V. Klein, T. N. Krabach, T. C. McGlinn, L. T. Ramano, and S. I. Shah, in *Proceedings of the 17th International Conference on the Physics of Semiconductors,* edited by J. D. Chadi and W. A. Harrison (Springer-Verlag, New York, 1985), p. 961.
[24]K. K. Tiong, P. M. Amirtharaj, F. H. Pollak, and D. E. Aspnes, Appl. Phys. Lett. **44**, 122 (1984).
[25]S. I. Shah, B. Kramer, S. A. Barnett, and J. E. Greene, J. Appl. Phys., **59**, 1482 (1986).
[26]O. S. Heavens, in *Physics of Thin Films,* edited by G. Haas and R. E. Thun (Academic, New York, 1964), Vol. 2, p. 193.
[27]J. I. Pankove, *Optical Processes in Semiconductors* (Dover, New York, 1971).
[28]J. A. Van Vechten and T. K. Bergstresser, Phys. Rev. B **1**, 3551 (1970).
[29]F. H. Pollak and R. Tsu, Proc. SPIE **452**, 26 (1983), and references therein.
[30]H. Kawamura, R. Tsu, and L. Esaki, Phys. Rev. Lett. **29**, 1397 (1972).
[31]W. B. Lacina and P. S. Perhsan, Phys. Rev. B **1**, 1765 (1970).
[32]Included in **p** is the scalar product of the polarizability tensor with unit polarization vectors for incident and scattered photons. See the equation preceding Eq. (49) of Ref. 31.
[33]J. Elliot, J. A. Krumhansl, and P. L. Leath, Rev. Mod. Phys. **46**, 465 (1974).
[34]R. I. Bonneville, Phys. Rev. B **29**, 907 (1984).